EUROFUSION WPMST2-PR(16) 14982

Jiri Adamek et al.

Fast measurements of the electron temperature and parallel heat flux in ELMy H-mode on the COMPASS tokamak.

Preprint of Paper to be submitted for publication in Nuclear Fusion

This work has been carried out within the framework of the EUROfusion Consortium and has received funding from the Euratom research and training programme 2014-2018 under grant agreement No 633053. The views and opinions expressed herein do not necessarily reflect those of the European Commission.

Fast measurements of the electron temperature and parallel heat flux in ELMy H-mode on the COMPASS tokamak

J Adamek[1], J Seidl[1], M Komm[1], V Weinzettl[1], R Panek[1], J Stöckel[1], M Hron[1], P Hacek[1], M Imrisek[1], P Vondracek[1], A. Devitre[2] and the COMPASS team

[1] Institute of Plasma Physics AS CR, Prague, Czech Republic

[2] Centro de Investigación en Ciencias Atómicas Nucleares y Moleculares, Universidad de Costa Rica

E-mail: adamek@ipp.cas.cz

Keywords: COMPASS, divertor, ELM, scrape-off layer, ball-pen probe, power decay length

Abstract. We report the latest results on fast measurements of the electron temperature and parallel heat flux in the COMPASS tokamak scrape-off layer (SOL) and divertor region during ELMy H-mode plasmas. The system of ball-pen and Langmuir probes installed on the divertor target, the horizontal reciprocating manipulator and the fast data acquisition system with sampling frequency rate f = 5 MSa/s allow us to measure the electron temperature and parallel heat flux during inter-ELM and ELM periods with high temporal resolution. The filamentary structure of the electron temperature and parallel heat flux was observed during ELMs in the SOL as well as in the divertor region. The position of the filaments within ELMs is not regular and therefore the resulting conditionally averaged ELM neglects the peak values of the electron temperature and parallel heat flux. We have found substantial difference between the value of the radial power decay length in the inter-ELM period $\lambda_{q,inter}$ = 2.5 mm and the decay length of the peak ELM heat flux $\lambda_{q,ELM}$ = 13.1 mm. Decay length of the total ELM energy $\lambda_{E,ELM}$=5.4 mm was found much smaller than that of the peak ELM heat flux.

1. Introduction

Investigation of the electron temperature and consequent parallel heat flux to the divertor target or to the first wall during Edge Localized Modes (ELMs) is of importance for the ITER tokamak in order to determine the physical sputtering and melting of the plasma facing compo-

nents [1, 2] and, consequently, their life time. The parallel heat flux $q_{//}$ can be determined using the formula $q_{//} = \gamma \cdot T_e \cdot I_{sat\_i}/S$, where T_e and I_{sat} are measured values of the electron temperature and ion saturation current, respectively. The coefficient γ represents the value of the heat power transmission coefficient [3] and S is the effective probe surface. Measurements of the ion saturation current during ELMy H-modes can be provided with a high temporal resolution using a Langmuir probe with surface S_{LP}, biased sufficiently negative with respect to its floating potential and expected electron temperature. On the other hand, fast measurements of the electron temperature during ELMy H-modes with microsecond temporal resolution are more difficult to achieve. The electron temperature in a divertor region of present-day devices is typically measured by swept Langmuir probes, which can also be used to investigate ELMs via fitted conditionally averaged *I-V* characteristics [4, 5] or a triple probe technique. The triple probe technique applied on Langmuir probes installed in the JET divertor can provide the electron temperature, density and heat flux with time resolution of 100 μs [6]. However, a large distance between the probes and required electronics per each triple probe limit the time resolution. Another limitation for use of the triple probe technique during ELMs is that the applied voltage V_{bias} should be much higher than the measured electron temperature T_e [7].

An alternative option to determine the electron temperature with a high temporal resolution is to use direct measurements of the plasma (Φ) and floating (V_{fl}) potentials. The electron temperature T_e is consequently determined from the difference of both potentials normalized by the proper coefficient for a specific gas and magnetic field [8, 9, 10]. The floating potential is routinely measured by a Langmuir probe (LP) and the plasma potential can be directly measured by a ball-pen probe (BPP) originally developed by Adamek et al. in IPP Prague and used on the CASTOR tokamak [10, 11]. The BPP has later been used to measure the plasma potential in the edge plasma of other fusion devices such as COMPASS [9, 12, 13], ASDEX Upgrade [8, 9, 13, 14, 15, 16], MAST [17] and ISTTOK [18] as well as in low-temperature magnetized plasmas [19, 20]. Recently, a new array of BPPs and dome-shaped Langmuir probes was installed in a divertor target of the COMPASS tokamak.

This paper reports the latest measurements of the parallel heat flux on the divertor target and at the low-field side (LFS) midplane during ELMy H-modes on the COMPASS tokamak. First, we describe the diagnostic set-up in Section 2 and discuss validity of the plasma potential measurement at the divertor in Section 3. Section 4 presents the first sub-microsecond measurement of the parallel heat flux during Type-I ELMs at the divertor and the same type of

measurement is repeated in Section 5 for the LFS midplane. Section 5 further compares power decay length during ELMs and in the inter-ELM periods.

2. BPP and LP construction and experimental set-up

The new array of BPPs (labelled A to L) has been implemented directly to the graphite divertor tile on the COMPASS tokamak as shown in figure 1. Each ball-pen probe is made of a stain-less-steel collector with 3 mm diameter and a boron-nitride shielding tube with 6 mm diameter. The collector is retracted at $h \sim 0.7$ mm below the graphite surface. Two additional dome-shaped LPs (Q, N) are also mounted on the same divertor target. The LPs are made of graphite with 4 mm diameter and protruding 1.3 mm into the plasma. Toroidal distance between neighbouring LPs is roughly 6 cm and is approximately the same between the BPP_H and LP_Q. In the current configuration, a set of probes BPP_H, LP_Q, LP_N is located at the same poloidal position. The Langmuir probes can operate in floating or ion saturation current modes (V_{bias} = -270 V). The total exposed area of LP is approximately S_{LP} = 30 mm^2. All signals are acquired with a sampling frequency rate f = 5 MSa/s. The BPPs are implemented to the divertor target as flush-mounted probes, which significantly reduce a direct impact of high heat flux on the probe material. The red lines show roughly a position of the strike points at HFS and LFS during the ELMy H-mode discharge #7891 at t = 1100ms.

At the midplane, the fast reciprocating probe shaft is used to insert a probe head containing BPPs and LPs, as seen on figure 2. On the COMPASS tokamak, measurements of the plasma and floating potential were performed by means of the central BPP2 with a retraction depth of h

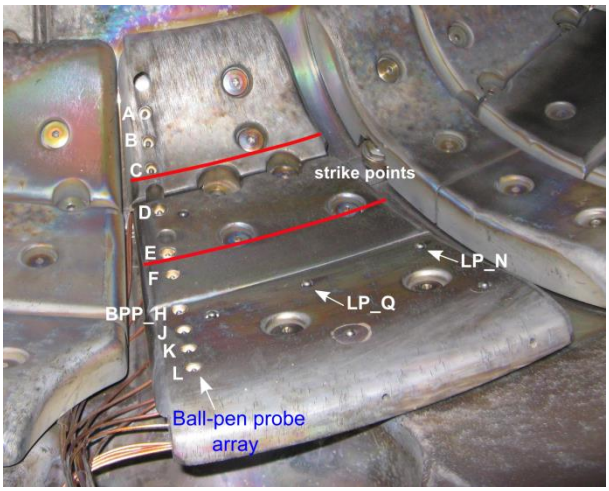

Figure 1 Picture of the ball-pen probe (BPP) array and dome-shaped Langmuir probes (LPs) mounted on the divertor target in COMPASS. The toroidal distance between BPP_H and LP_Q and neighbouring LPs is roughly 6 cm. The red lines shows the approximate po-sition of the strike points at HFS and LFS in shot #7891 at t=1100 ms.

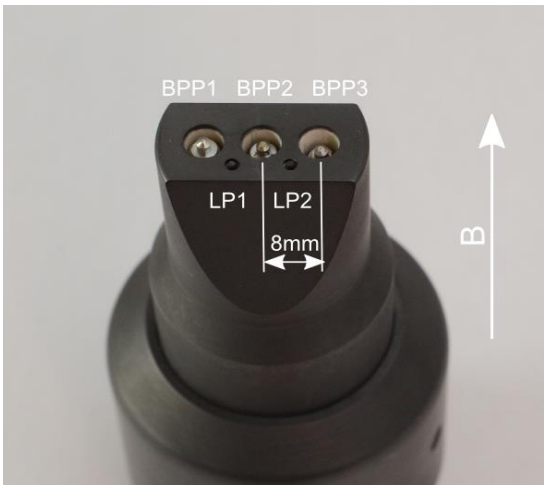

Figure 2 Picture of the ball-pen probe head used on the COMPASS midplane manipulator. It consists of three ball-pen probes with stainless steel collectors and alumina shielding tubes and two graphite Langmuir probes.

= –0.5 mm and Langmuir probe LP1. The ion saturation current I_{sat_i} is provided by LP2 (V_{bias} = -270 V). The diameter of the probe head is about 3 cm on the top. The ball-pen probes have stainless steel collectors with diameter of 2 mm and alumina shieldings with inner diameter of 5 mm. The LPs are made of graphite pins with diameter of 0.9 mm protruding 1.5 mm into the plasma (the same construction is used on ASDEX Upgrade). The poloidal distances between the LPs and BPPs are 4 mm. All signals are acquired with a sampling frequency rate f = 5 MSa/s.

3. Characteristics of divertor BPP

Current-voltage characteristics of BPPs mounted on the probe manipulators have been systematically studied in the SOL of different tokamaks such as ASDEX Upgrade [8], CASTOR [10, 11], ISTTOK [18], TJ-K [20] and low temperature plasma devices [19, 20]. The idea of the BPP to directly measure the plasma potential is based on the simple Langmuir probe theory for Maxwellian plasma. It predicts that, if the ratio $\mathcal{R} = I_{sat\_e}/I_{sat\_i}$ of the electron and ion saturation current is equal to one, the floating probe potential is equal to the plasma potential Φ. Thus, the floating ball-pen probe potential Φ^{BPP} is close to the plasma potential Φ. The ratio $\mathcal{R}$ is rendered approximately one due to the screening of a large portion of electrons from reaching the collector by its ceramic shielding [8, 10]; and also the *I-V* characteristics of BPP becomes nearly symmetric. We have also performed comparative measurements of BPP and self-emitting Langmuir probe in SOL on COMPASS [13] and ASDEX Upgrade [13] with a good agreement of both techniques.

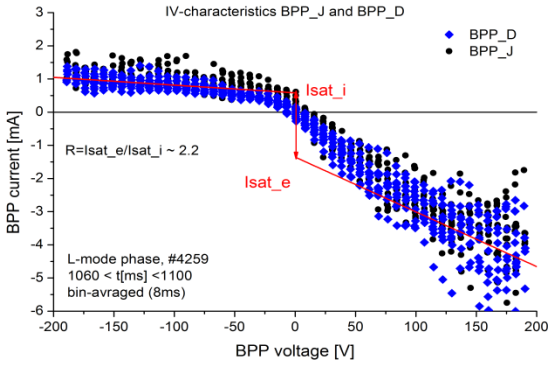

Figure 3: *I-V* characteristics of BPP_D (blue) and BPP_J (black) during the whole L-mode phase of H-mode discharge #4259.

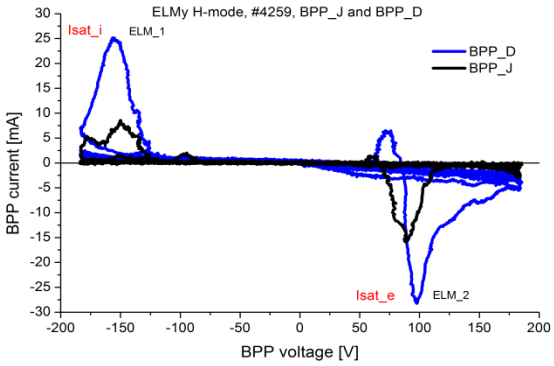

Figure 4: *I-V* characteristics of BPP_D and BPP_J during ELMy H-mode phase #4259 with two similar ELM events incoming to both probes.

The BPPs at the divertor are surrounded by large graphite (conducting) tiles, which is a new probe arrangement in contrast to the BPP mounted on the probe manipulator as seen in figure 2. Therefore, in order to verify symmetry of *I-V* characteristics of divertor BPPs, we have applied swept voltage (+/-200 V, f = 1 kHz) on two BPPs (BPP_J, BPP_D) with significantly different

poloidal locations. For each probe, an example of the resulting *I-V* characteristics obtained during the L-mode phase (B_T = 1.15 T, plasma current I_P = 200 kA, density $n_e = 6 \cdot 10^{19}$ m^{-3}) of H-mode discharge #4259 is plotted in figure 3. It can be seen that both probes provide nearly symmetric *I-V* characteristics during the whole time interval. It is also seen that electron and ion branch of the *I-V* does not saturate, and therefore the evaluation of the ratio of the electron and ion saturation current $\mathcal{R} = I_{sat\_e}/I_{sat\_i}$ requires a linear extrapolation of both branches to V_{fl}. The linear fit in figure 3 is calculated for BPP voltage > +100 V in the electron branch and for BPP voltage < -100 V in the ion branch. If we assume the floating potential of BPP is close to the plasma potential Φ, then the logarithm of the ratio $\mathcal{R}$ is found to be close to $\ln(\mathcal{R}) \sim 0.8$. The resulting value $\ln(\mathcal{R})$ is close to the value obtained with BPPs mounted on a probe manipulator on AUG [2].

Determination of the ratio $\mathcal{R}$ during ELMs is difficult because of a very short time scale of ELM filaments compared with the sweeping period. However, raw estimation of the ratio between the electron and ion saturation current during an ELMs is shown in figure 4. Two similar ELM events, ELM_1 and ELM_2, with the same D-alpha footprint, were detected on swept BPP_J and BPP_D during ELMy H-mode phase of the discharge #4259 ($n_e = 9 \cdot 10^{19}$ m^{-3}) at moments with opposite values of applied voltage. This confirms that both values I_{sat_e} and I_{sat_i} are also roughly balanced within the ELM, with the ratio $1 < \mathcal{R} < 2$ independent on the probe position. Note, the investigation of the ratio $\mathcal{R}$ of BPP during ELMy H-mode can be also found in systematic measurements on ASDEX Upgrade [8]. The investigation of the electron temperature T_e with a microsecond temporal resolution is based on fast measurements of BPP and LP potentials, Φ^{BPP} and V_{fl}, and on the formula $T_e = (\Phi^{BPP} - V_{fl})/2.2$ [9] The coefficient 2.2 is obtained from the $\ln(\mathcal{R}) = 2.8$ of LP in deuterium plasmas (assuming $T_i = T_e$ and no secondary electron emission) minus the $\ln(\mathcal{R})$ of BPP. The value of $\ln(\mathcal{R})$ of BPP on COMPASS (shown in figure 3 and figure 4) is in agreement with the value $\ln(\mathcal{R})$ achieved on ASDEX Upgrade [8]. Therefore, we shall use the same value of $\ln(\mathcal{R}) = 0.6$ for BPPs on both COMPASS and ASDEX Upgrade. Note, the same formula was already used for comparative measurements of the electron temperature using BPP/LP mounted on the reciprocating manipulator and Thomson scattering on COMPASS [9], ASDEX Upgrade [9] and MAST [17] in L-mode plasmas with a very good agreement of both techniques.

4 Fast measurements of ELMs in divertor region

The combination of BPP_H (Φ^{BPP}) and LP_Q (V_{fl}) in a floating regime and LP_N (biased with V_{bias} = -270 V) allow us to provide simultaneous measurements of the electron temperature T_e from Φ^{BPP} and V_{fl} and ion saturation current I_{sat_i} on the LFS roughly at the R-$R_{strike\ point}$ ~ 6 cm, as seen in figure 1. An example of the temporal evolution of the electron temperature and ion saturation current during a type-I ELM in discharge #7891 is plotted in figure 5.

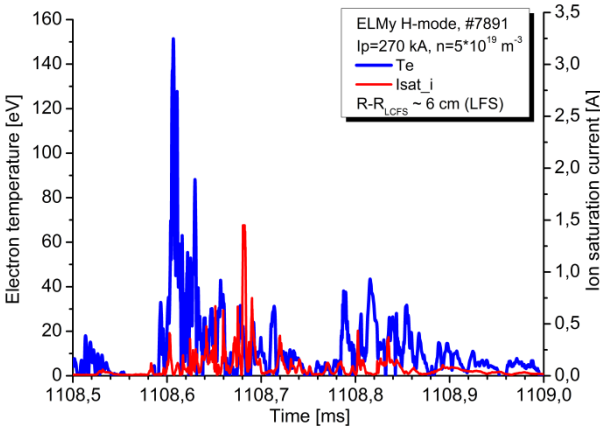

Figure 5: Temporal evolution of the electron temperature and ion saturation current during a single ELM event in H-mode #7891 (I_p=270 kA, n=5·10^{19} m^{-3}) in the COMPASS divertor region.

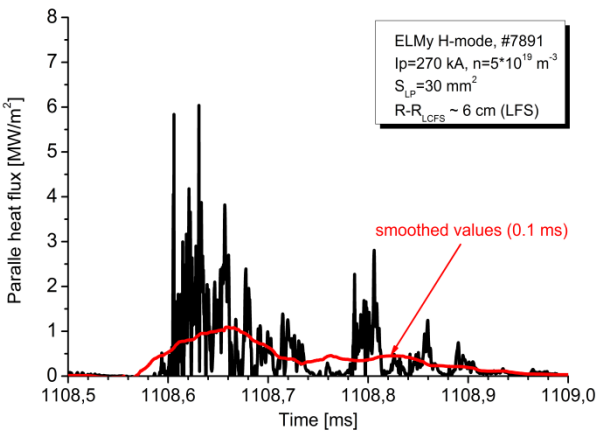

Figure 6 Temporal evolution of the parallel heat flux obtained from T_e and I_{sat_i} measurements and heat transmission coefficient γ=7 during the same ELM event, as in figure 5 in shot #7891.

It is seen that the value of the electron temperature is strongly varying within an ELM structure and not correlated with the time evolution of the ion saturation current. It must be noted, that a small part of the resulting T_e, roughly 9% of the total signal during the H-mode phase, has values below zero, because in some cases it is observed that signals of Φ^{BPP} and V_{fl} are slightly shifted in time during ELM filaments, and therefore their difference is unphysically negative. This can be caused by a small misalignment of the BPPs and LPs with respect to the magnetic field lines or by different dimensions of each probe. However, the major part of T_e values can be used in order to estimate the value of the parallel heat flux $q_{//}=\gamma \cdot T_e \cdot I_{sat\_i}/S_{LP}$, where we have used γ = 7 [3] and S_{LP} = 30 mm^2 is the total exposed surface of LP_N. The time evolution of $q_{//}$ during one ELM is plotted in figure 6. It is seen that the value of the parallel heat flux during ELMs reaches several MW/m^2. These values are obtained roughly 6 cm outside the LFS strike point. The red line represents smoothed values of the parallel heat flux over 0.1 ms (10 kHz), which is comparable to the resolution of common IR cameras. In such case, the resulting values of $q_{//}$ are below 1 MW/m^2 and strongly underestimate the peak heat flux.

Figure 6 shows that an ELM is composed of several high heat flux filaments separated by periods of a low heat flux. It has been found that the position of the filaments within one ELM is, however, not regular as it is also seen in measurements at midplane plotted in figure 8. This

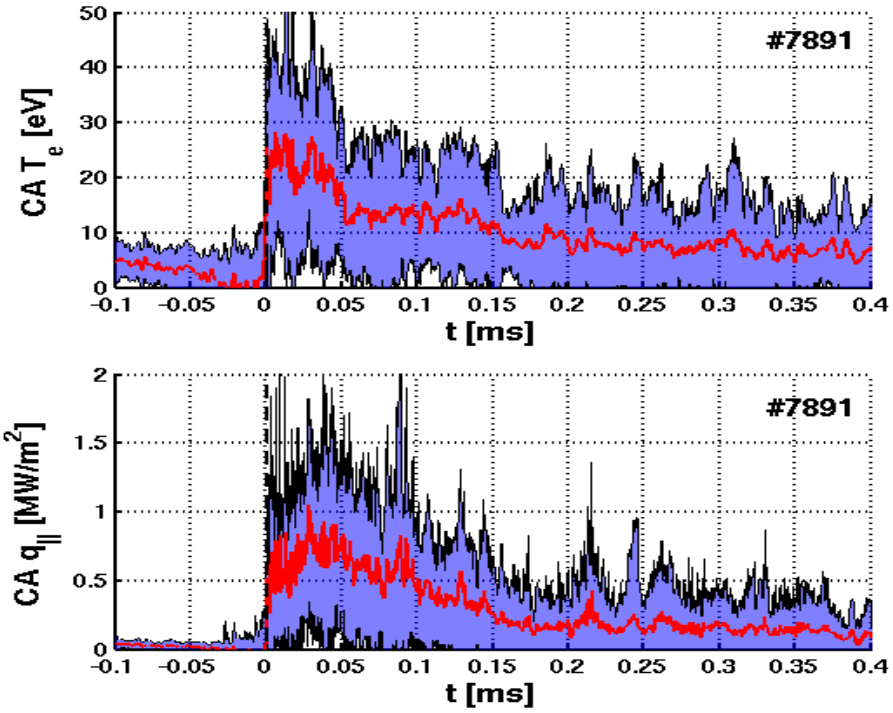

Figure 7 Conditionally averaged electron temperature (CA T_e) and parallel heat flux (CA $q_{//}$) in type-I ELM (red line) is calculated from 30 ELM events during the ohmic H-mode #7891(I_p=270 kA, n=5·10^{19} m^{-3}) at LFS roughly at R-$R_{strike\ point}$ ~ 6 cm. The blue line represents +/- 1 σ of standard deviation.

can be demonstrated by computing a conditionally averaged (CA) ELM waveform. For each ELM, the heat flux signal is extracted from the time window $0.1 < t\text{-}t_{front}$ [ms] < 0.4 and all such signals are averaged together. Here t_{front} is the time of the initial steep increase of the heat flux representing the time when the first filament of ELM hits the probe position. The value t_{front} is determined at the time when the heat flux exceeds a predefined threshold $q_{//thr}$ for the first time. There, $q_{//thr}$ is set larger than the maximum of the heat flux in the inter-ELM phase.

The resulting conditionally averaged ELM waveform on the divertor is plotted by as a red line in figure 7. The blue line represents +/- 1 σ of standard deviation. The filamentary structure of CA T_e and CA $q_{//}$ ELM has disappeared after the conditional averaging due to an irregular filamentary structure of each ELM. It is also clearly seen that the maximum value of the $q_{//}$ in CA ELM in figure 7 is significantly lower than the peak heat flux of individual filaments. This demonstrates that techniques that use an ensemble averaging for a description of the heat flux within unsorted ELMs, such as the conditional averaging of an I-V characteristic [4, 5], will also tend to underestimation of the maximum heat flux.

5 ELM filamentary structure and decay length in SOL

The fast reciprocating probe shaft on the COMPASS midplane manipulator [13, 21] is used to measure the electron temperature [3], ion saturation current and parallel heat flux in L-mode as well as in ELMy H-mode discharges. The data are measured with a microsecond temporal resolution, which allows us to resolve the filamentary structure of ELMs. The electron temperature is provided by a combination of BPP2 and LP1 values as seen in figure 2 using the same formula $T_e=(\Phi^{BPP} - V_{fl})/2.2$ as in the case of the divertor measurements. The ion saturation

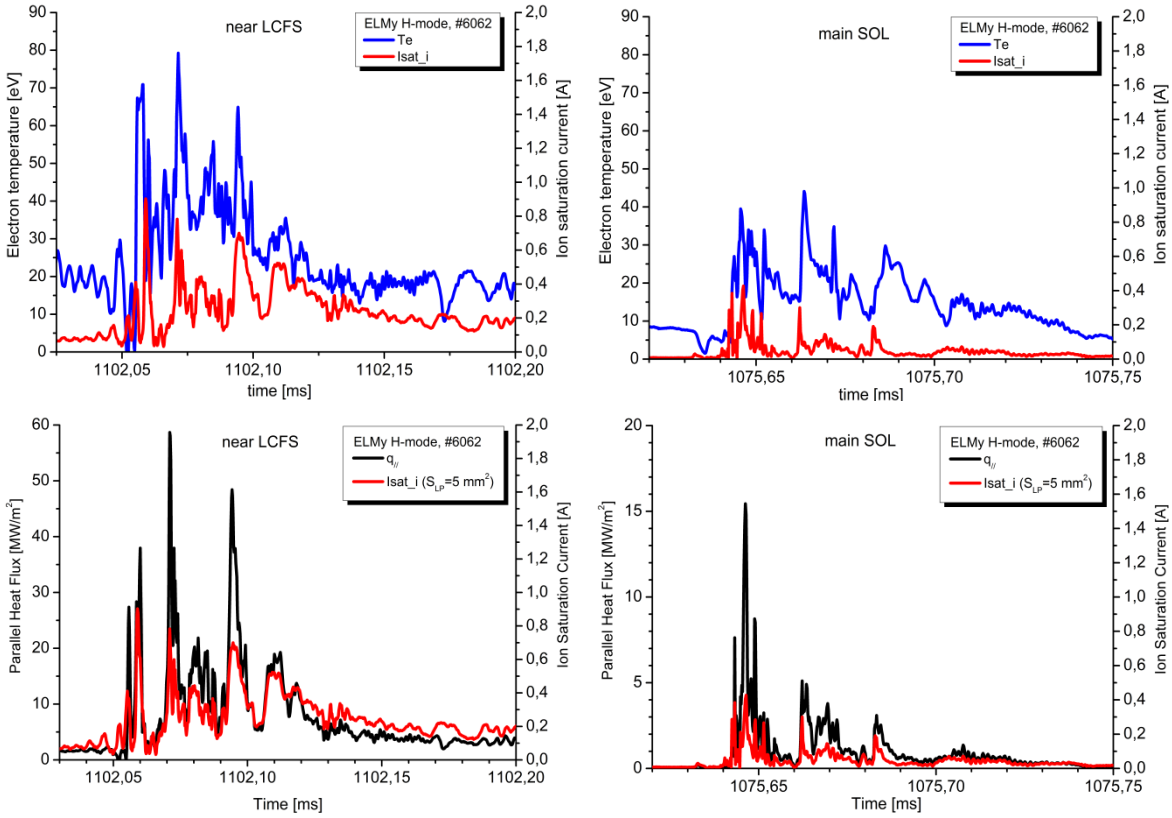

Figure 8 Temporal evolution of the electron temperature, ion saturation current and parallel heat flux during single ELM events near the LCFS (left) and in the main SOL (right) in shot #6062 (I_p=270 kA, n=5·10^{19} m^{-3}).

current is provided by LP2 with the total exposed area of approximately S_{LP} = 5 mm^2, the parallel heat flux is calculated with the same value of the heat power transmission coefficient γ= 7 as in the divertor measurements. Temporal evolution of the electron temperature, ion saturation current and parallel heat flux of two similar ELM events measured by probes at two different positions is plotted as an example in figure 8. Both measurements near the LCFS and in the main SOL clearly show several filaments, in which the electron temperature and ion saturation current are in phase. Consequently, these filaments will dominate the resulting parallel heat flux. Although the values of the peak heat flux decrease with the distance from LCFS, it would always significantly exceeds the smoothed or conditionally averaged value of T_e or $q_{//}$ within the

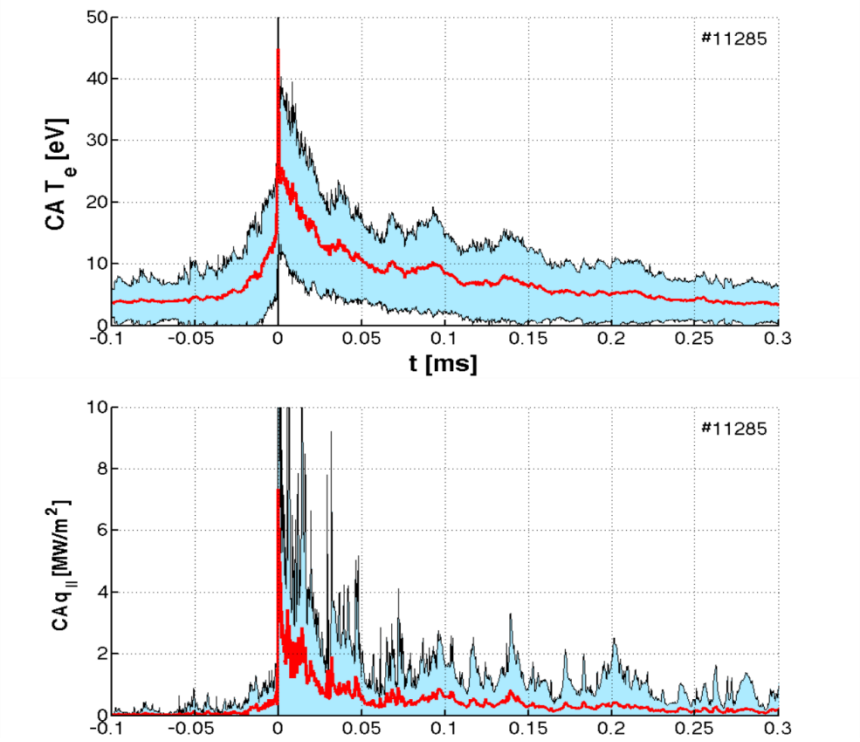

Figure 9 Conditionally averaged electron temperature (CA T_e) and parallel heat flux (CA $q_{//}$) of type-I ELM (red line) is calculated from 51 similar ELM events during the flat-top in shot #11285 (I_p=300 kA, n=6·10^{19} m^{-3}). The blue line represents +/- 1 σ of standard deviation.

ELM. Systematic measurements of the electron temperature and parallel heat flux in the ELMy H-mode discharge #11285 at the first wall are shown in figure 9.

Position of the probe head on the midplane manipulator was fixed at 10 mm in front of the LFS limiter during the whole discharge in order to obtain conditionally averaged ELM characteristics. During the ELMy H-mode phase we measured 51 ELMs events with a similar H-alpha footprint yielding the resulting CA ELM evolution. The same method of CA was used as for the divertor measurements in the previous chapter. The final conditionally averaged ELM is plotted in figure 9 as a red line. The blue region represents +/- 1 σ of the standard deviation. The filamentary structure of T_e and $q_{//}$ inside the ELM has again disappeared after the conditional averaging due to a different structure of each ELM. It is also clearly seen that the maximum value of $q_{//}$ in the CA ELM in figure 9 is significantly lower than the peak heat flux of individual filaments.

BPPa and LPs mounted on the reciprocating manipulator allow us to perform fast measurements of $q_{//}$ at different radial positions during a single ELMy H-mode discharges. By separating subsets of data that belong to ELMs and inter-ELM periods, respectively, we can evaluate the power decay length λ_q of the inter-ELM plasma and compare it with the decay length of the peak ELM heat-flux.

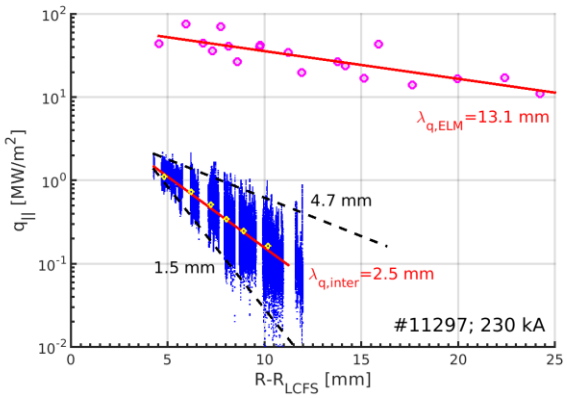

Figure 10 Radial profile of parallel heat flux during inter-ELM period (blue dots) and peak heat flux of type-I ELMs (violet/pink circles) during the ohmic H-mode discharge #11297 (I_p=230 kA, n=7·10^{19} m^{-3}). Yellow circles show an averaged heat flux in each individual inter-ELM period.

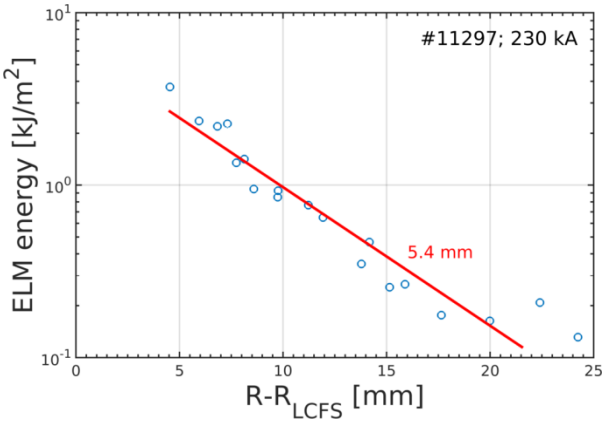

Figure 11 The radial profile of total energy of each ELM in shot #11297 (I_p=230 kA, n=7·10^{19} m^{-3}).

The resulting profiles of $q_{//}$ obtained during the ohmic ELMy H-mode discharge #11297 with I_p=230 kA and n=7·10^{19} m^{-3} are plotted in figure 10 with respect to the position of LCFS. The low field side limiter is located roughly 40 mm far from LCFS. The blue dots represent measured values of the parallel heat flux during inter-ELM periods. Fit of the values by the exponential function $q_{//}(R\text{-}R_{\mathrm{LCFS}}) = q_{//,0}\exp(-(R\text{-}R_{\mathrm{LCFS}})/\lambda_q)$ shown as a red line gives the averaged value of the inter-ELM power decay length $\lambda_{q,inter}$ = 2.5 mm. This fit agrees well also with the mean heat flux evaluated separately for each inter-ELM period (yellow circles). The fluctuating part of the inter-ELM heat flux is approximately bounded by lower and upper value of the power decay length at 1.5 mm and 4.7 mm. The value of the averaged profile $\lambda_{q,inter}$ is the best candidate to be compared with slower measurements by means of the IR camera, which were systematically carried out for several major tokamaks in [22]. The Eich scaling [22] predicts for our discharge #11297 the value of the inter-ELM power decay length $\lambda_{q,Eich}(\#9)$ = 1.8 mm or, including the spherical tokamaks, $\lambda_{q,Eich}(\#14)$ = 3.3 mm. The experimental value $\lambda_{q,inter}$ = 2.5 mm found for COMPASS is within the range of these two predicted values. We can determine the power decay length of ELMs as well. The maxima of $q_{//}$ of each ELM with respect to the probe position are plotted in figure 10 by magenta circles. It again shows an exponential decay, however the value of the power decay length $\lambda_{q,ELM}$ = 13.1 mm is roughly 5 times higher than that determined from the inter-ELM measurement. This indicates that the peak heat flux carried by ELMs on the midplane is significantly less reduced by transport across field lines than the inter-ELM heat flux and may have a strong impact on the first wall. The material of the first wall will be sputtered not only due to the incoming peak heat flux but also due to the total en-

ergy of the ELM. Therefore, we have evaluated the total energy of each ELM as an integral of the measured heat flux over the period of ELM duration (see figure 11). It is seen that the total energy decay length $\lambda_{E,ELM}$ =5.4 mm is much smaller than the power decay length of the peak heat flux $\lambda_{q,ELM}$ = 13.1 mm.

6 Summary

Fast measurements of the electron temperature and parallel heat flux were performed in the SOL and divertor region of the COMPASS tokamak using the ball-pen and Lagmuir probe techniques with a sub-microsecond temporal resolution. The divertor target was recently equipped with an array of ball-pen and Langmuir probes in order to measure the parallel heat flux in the LFS. The measurements in SOL were performed using a standard probe head equipped with ball-pen and Lagnmuir probes operating on a midplane reciprocating manipulator. The systematic measurements in ELMy H-modes show a clear filamentary structure of electron temperature, density and resulting parallel heat flux during ELMs in SOL as well as in the divertor region. However, the number and positions of filaments within ELMs are not regular and therefore the resulting conditionally averaged ELM neglects the peak heat flux as it was shown for the case of the divertor region and the vicinity of the first wall in SOL. Values of the peak heat flux in ELMs are always significantly higher than conditionally averaged ELM values and can be obtained only with diagnostics with a microsecond temporal resolution. The power decay length was measured during both the inter-ELM and ELM periods in shot #11297. It was found that the power decay length of the inter-ELM averaged profile of the parallel heat flux is $\lambda_{q,inter}$ = 2.5 mm. The value is just in the range of predicted by the of Eich scaling, $\lambda_{q,Eich}(\#9)$ = 1.8 mm or $\lambda_{q,Eich}(\#14)$ = 3.3 mm. However, the radial profile of the peak heat flux of ELMs provides the power decay length $\lambda_{q,ELM}$ = 13.1 mm, which is roughly 5 times higher than its inter-ELM value. This means that the peak heat flux within ELMs is less reduced by the cross-field transport than the inter-ELM heat flux. This can be caused by a high radial velocity of ELMs. The peak heat flux can strongly influence the local heating of the top layer of the material of the first wall or divertor target. However, heating of the material by ELMs is proportional to the energy of each ELM. Therefore, we have studied radial profiles of the energy of ELMs and found that the decay length of the ELM energy is $\lambda_{E,ELM}$=5.4 mm, which is less than the decay length of the peak heat flux $\lambda_{q,ELM}$ = 13.1 mm.

This means that the total energy of each ELM, which will heat the material of the first wall, is less “dangerous” than the local (in time) impact of peak heat flux of ELMs. The final sputtering

of the thin top layer of material of the first wall or divertor target will depend on the duration of the filaments and its peak heat flux and the thermal conductivity of the material.

Acknowledgements

This work was supported by the project of the Czech Science Foundation GA15-10723S and MSMT Project #LM2011021. It has been carried out within the framework of the EUROfusion Consortium and has received funding from the Euratom research and training programme 2014-2018 under grant agreement No 633053. The views and opinions expressed herein do not necessarily reflect those of the European Commission.

References

[1] J.W. Coenen et al., Nuclear Fusion 55 (2015) 023010.

[2] G. Arnoux, et al., J. Nucl. Mater. 463, (2015) 415–419.

[3] J.G. Watkins et al., J. Nucl. Mater. 390–391 (2009) 839–842.

[4] C Guillemaut et al., Plasma Phys. Control. Fusion 57 085006 (2015).

[5] C Guillemaut et al., Physica Scripta T167 (2016) 014005.

[6] S. Jachmich et al., 36th EPS Conference on Plasma Phys., Sofia, P-2.159 (2009).

[7] D. Tskhakaya, S. Jachmich, T. Eich, W. Fundamenski, J. Nucl. Mater. 415 (2011) S860–S864.

[8] J. Adamek et al., Contrib. Plasma Phys. 50, (2010) 854.

[9] J. Adamek, et al., 41st EPS Conference on Plasma Physics, Berlin, P2.011 (2014).

[10] J. Adamek et al., Czech. J. Phys. 54, C95-C99 (2004).

[11] J. Adamek et al., Czech. J. Phys. 55, 235 (2005).

[12] R. Panek et al., Plasma Phys. Control. Fusion 014015 **58**: 014015.

[13] J. Adamek et al., Contrib. Plasma Phys. 54, No. 3, 279 – 284 (2014).

[14] H. W. Müller et al., Nuclear Fusion 51, 073023 (2011).

[15] J. Horacek et al., Nuclear Fusion 50, 105001 (2010).

[16] J. Adamek et al., J. Nucl. Mater. 390–391 (2009) 1114–1117

[17] N. R. Walkden et al., Review of Scientific Instruments 86, 023510 (2015).

[18] C Silva et al., Plasma Phys. Control. Fusion 57 (2015) 025003.

[19] M. Zanaska et al., Phys. Plasmas 22, 033516 (2015).

[20] J. Adamek et al., Contrib. Plasma Phys. 53, (2013) 39–44.

[21] V. Weinzettl et al., Fusion Engineering and Design 86 (2011) 1227–1231

[22] T. Eich et al., Nuclear Fusion 53 (2013) 093031.